Available online at www.sciencedirect.com

SciVerse ScienceDirect

Journal of the European Ceramic Society 33 (2013) 413–421

www.elsevier.com/locate/jeurceramsoc

The effect of a graphite addition on oxidation of ZrB_2–SiC in air at 1500 °C☆

Alireza Rezaie *[,1], William G. Fahrenholtz [1], Gregory E. Hilmas [1]

Department of Materials Science and Engineering, Missouri University of Science and Technology, Rolla, MO 65409, USA

Received 23 April 2012; received in revised form 15 September 2012; accepted 19 September 2012
Available online 7 October 2012

Abstract

Dense ZrB_2 containing 15 vol.% SiC and 15 vol.% graphite was exposed to flowing air at 1500 °C. A layered scale structure developed that consisted of (1) a uniform SiO_2-rich layer on the surface, (2) a layer of ZrO_2 and SiO_2, (3) a layer of ZrO_2 (4) a partially oxidized layer composed of porous ZrB_2, ZrO_2, and graphite, and (5) unaffected ZrB_2–SiC–C. A thermodynamic model based on volatility diagrams and consistent with the experimental observations was constructed to explain the development of the layered structure. Oxidation behavior was consistent with passive oxidation and formation of a protective surface layer. Analysis indicated that it may not be possible to form a protective surface layer without actively oxidizing SiC and producing a porous partially oxidized layer between the outer protective layer and the underlying unoxidized material.

Keywords: ZrB_2; SiC; Oxidation; Carbon; Thermodynamic model

1. Introduction

Ultra high temperature ceramics (UHTCs) are a group of compounds that generally consists of carbides (TaC, ZrC, HfC), borides (ZrB_2, HfB_2) and nitrides (HfN) of the early transition metals. UHTCs have recently attracted significant research interest due to potential applications in thermal protection systems (TPSs) for hypersonic aerospace vehicles and reusable atmospheric re-entry vehicles.[1–12] UHTCs can potentially be used at temperatures above 1500 °C in oxidizing environments. The combination of desired properties such as high melting temperature (>3000 °C) and strength at elevated temperature make UHTCs attractive candidates for hypersonic flight, atmospheric re-entry, and rocket propulsion applications, which have harsh thermal and chemical environments. Because it has the lowest theoretical density (6.09 g/cm^3) among UHTCs and good resistance to thermal shock due to its high thermal conductivity (65–135 W/m K), ZrB_2 is an outstanding candidate for aerospace applications.[13]

Oxidation of ZrB_2 and ZrB_2-based ceramics has been studied by a number of investigators.[14–17] When exposed to air, ZrB_2 undergoes stoichiometric oxidation to form crystalline ZrO_2 and B_2O_3 (l).[18,19] The B_2O_3 (l) is an effective barrier to the transport of oxygen, leading to passive oxidation behavior with parabolic mass gain kinetics.[16] Rapid evaporation of B_2O_3 (l) at temperatures above 1100 °C reduces the effectiveness of the diffusion barrier because the ZrO_2 that is left behind has a porous structure and does not protect the underlying ZrB_2 from further oxidation.[20] Between 1100 °C and 1400 °C, para-linear kinetics have been observed since the rate of B_2O_3 (l) vaporization is comparable to the rate of formation of B_2O_3 (l). In this temperature regime, the overall rate of mass change is a combination of mass gain due to oxidation and mass loss due to B_2O_3 (l) vaporization.[8,21] At temperatures above ~1400 °C, ZrB_2 exhibits linear mass gain kinetics (passive oxidation but a non-protective oxide scale of ZrO_2) because the rate of B_2O_3 vaporization is rapid compared to its rate of formation.[22]

A number of additives have been used to improve the oxidation resistance of ZrB_2-based materials.[23–26] The addition of SiC improves oxidation resistance at temperatures above 1200 °C by promoting the formation of a borosilicate glass layer, which reduces oxygen permeability on exposed surfaces. The layer provides passive oxidation behavior resulting in parabolic mass

☆ This material is based upon work supported by the National Science Foundation under grant number DMR-0346800.

* Corresponding author. Current address: Vesuvius Research at 4604 Campbells Run Road, Pittsburgh, PA 15220, USA. Tel.: +1 412 505 6530; fax: +1 412 787 5718.
E-mail addresses: Alireza.rezaie@us.vesuvius.com, alireza_r76@yahoo.com (A. Rezaie).
[1] Member, American Ceramic Society.

0955-2219/$ – see front matter © 2012 Elsevier Ltd. All rights reserved.
http://dx.doi.org/10.1016/j.jeurceramsoc.2012.09.016

gain kinetics, which reduces the oxidation rate compared to pure ZrB_2.[25,27] The SiO_2-rich glassy scale remains protective up to at least 1600 °C on pure SiC.[27] For ZrB_2–SiC, the SiO_2 is significantly less volatile than B_2O_3 ($\sim 10^5$ times lower vapor pressure for SiO_2 than B_2O_3 at 1500 °C), resulting in passive oxidation protection over a much greater temperature range for ZrB_2–SiC than has been reported for pure ZrB_2.[21,27]

Exposure of ZrB_2–SiC to air at 1500 °C results in the formation of a layered surface structure that consists of four layers: (1) a continuous SiO_2-rich layer on the surface, (2) a layer of ZrO_2 and amorphous SiO_2, (3) a partially oxidized layer that is depleted of SiC, and (4) unaffected ZrB_2–SiC.[21] The partially oxidized layer consists of ZrB_2 or ZrO_2, depending on the pressure of oxygen across the layer. The structure of this layer is similar to the original ZrB_2–SiC, but with the SiC partially or fully removed. The conditions that lead to the formation of the partially oxidized layer depleted of SiC have been described by several investigators.[21,28–31] A thermodynamic model using volatility diagrams of ZrB_2 and SiC was used to explain the development of the layered structure and the SiC-depleted layer.[21] The model suggests that SiC below the outer silica layer undergoes active oxidation leading to the formation of the SiC-depleted region.[21,28] Because the outer SiO_2-rich scale acts as a diffusion barrier, the oxygen activity beneath the scale is much lower than in the surrounding air. Under the reducing conditions that exist beneath the outer SiO_2-containing layers, SiO (g) and CO (g) have high vapor pressures above SiC ($\sim 10^3$ Pa at 1500 °C), which leads to active oxidation of SiC.

The addition of graphite to ZrB_2–SiC may affect the formation of the SiC-depleted layer beneath the outer SiO_2-rich scale. Graphite increases the activity of carbon compared to nominally pure SiC, which should have a corresponding effect on the pressure of carbon monoxide below the SiO_2-containing layers. Consequently, the addition of carbon may inhibit the vaporization of SiC due to increased pressure of carbon monoxide. As a result, the total pressure of carbon monoxide in equilibrium with SiC beneath its outer SiO_2 layer is dependent upon the carbon activity of the system.[32] At ~1500 °C, the total pressure ($pSiO + pO_2$) has been reported to increase substantially (~100 times) for carbon saturated silicon carbide in contact with silica compared to nominally pure silicon carbide.[33]

The purpose of this paper is to describe the effect of the addition of graphite on the oxidation behavior of ZrB_2–SiC in air. The layered structure formed during oxidation in air at 1500 °C was characterized. A thermodynamic model was used to explain the development of the layered structure.

2. Experimental procedure

2.1. Processing

Commercial ZrB_2 (Grade B, H.C. Starck, Newton, MA) with an average particle size of 2 μm and reported purity of >99% was used. The SiC powder (Grade UF-10, H.C. Starck, Newton, MA) was predominantly α-SiC and had a purity of 98.5% and average particle size of 0.7 μm. The purity of graphite powder (Grade UFG-5, Showa Denko, Ridgeville SC) was >98% with an average particle size of 3.0 ± 1.5 μm. The overall batch composition was 84.0 wt% ZrB_2, 9.5 wt% SiC, and 6.5 wt% graphite, which corresponds to 70 vol% ZrB_2, 15 vol% SiC, and 15 vol% graphite based on densities of 6.09 g/cm^3 for ZrB_2, 3.21 g/cm^3 for SiC, and 2.20 g/cm^3 for graphite. The ZrB_2 and SiC were attrition milled (Model 01-HD, Union Process, Akron, OH) for 2 h at 600 rpm with the graphite added for the last 5 min of milling to allow it to mix, but to minimize its size reduction. Attrition milling, which reduced the particle size and promoted intimate mixing of the components, was performed in a 750 ml fluoropolymer-coated bucket containing ~250 ml hexane, ~150 g of the powder mixture, and ~3000 g of ZrO_2 milling media (~3.5 mm diameter spheres). For solvent removal, rotary evaporation (Model Rotavapor R-124, Buchi, Flawil, Germany) was employed at a temperature of 70 °C, a vacuum of 200 mm Hg (~27 kPa), and a rotation speed of 150 rpm.

Milled powder was loaded into a graphite die lined with graphite foil and coated with BN and then hot-pressed (Model HP-3060, Thermal Technology, Santa Rosa, CA). The furnace was heated at an average rate of ~10 °C/min using a temperature cycle that has been described in more detail previously.[34,35] Specimens were heated in vacuum (~20 Pa) up to 1650 °C, then the atmosphere was switched to flowing argon. Above ~800 °C, an infrared thermometer (Model OS 3708, Omega Engineering, Stamford, CT) monitored the temperature of the graphite die. When the die temperature reached the hold temperature of 1950 °C, a uniaxial load of 32 MPa was applied. The furnace was held at 1950 °C for 45 min and then cooled at ~20 °C/min to room temperature. The load was removed at ~1750 °C. For oxidation, bars with the dimensions of 64 mm × 4 mm × 4 mm were diced from the hot pressed billets.

2.2. Oxidation

The experimental portion of this study focused on exposing the ZrB_2–SiC–C specimens to air at 1500 °C. For the oxidation studies, a $MoSi_2$ resistance heated horizontal tube furnace (Model 0000543 Rapid Temperature Furnace, CM Inc., Bloomfield N.J.) equipped with a high purity alumina tube having an inside diameter of ~6.35 cm was used. Prior to oxidation, specimens were cleaned in acetone in an ultrasonic bath. Cleaned specimens were placed on an alumina plate, which was on an alumina D-tube, and then inserted into the center of the furnace and leveled. The ends of the tube were sealed with gas-tight end caps. A flowing air atmosphere with a flow rate of ~1.8 l/min was maintained. Specimens were heated at 5 °C/min to 1500 °C and held for times ranging from 0 to 8 h.

2.3. Characterization

Scanning electron microscopy (SEM; S-570, Hitachi, Tokyo, Japan) was used to characterize the microstructure of the oxidized specimens. Energy dispersive spectroscopy (EDS; AAT, X-ray Optics, Gainesville, FL) was employed for chemical analysis. Samples were prepared for microscopy by cutting cross sections, mounting them in epoxy, and then polishing

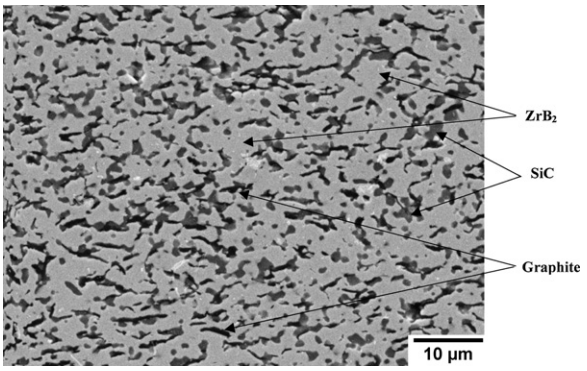

Fig. 1. A polished cross section showing the microstructure of a ZrB_2–SiC–C specimen prepared by hot pressing at 1950 °C for 45 min.

to a 0.25 μm finish with diamond abrasives. A specimen oxidized at 1500 °C for 8 h was examined using grazing incidence X-ray diffraction (GXRD; X'Pert MRD, Panalytical, Almelo, the Netherlands) to determine the crystalline phases that were present at various depths into the specimen. Polishing was used to remove the layers sequentially so that each could be examined by GRXD. Removal of the layers was monitored using optical microscopy so that the desired depth was reached. An incident angle of 1° was used to minimize the penetration of the X-ray beam into the specimen and thereby maximize the diffracted signal from the region of interest.

3. Results and discussion

3.1. Density and microstructure

The bulk density of the hot pressed billets used in this study was 5.01 g/cm^3. A volumetric rule of mixtures was used to calculate the theoretical density for ZrB_2–SiC–C. Assuming theoretical densities of 6.09 g/cm^3 for ZrB_2, 3.21 g/cm^3 for SiC, and 2.20 g/cm^3 for graphite, the theoretical density of ZrB_2 containing 15 vol% SiC and 15 vol% graphite was calculated to be 5.07 g/cm^3. Based on this true density, both billets were hot pressed to near theoretical density (>98%), with no indication of open porosity.

A microstructure representative of the ZrB_2–SiC–C specimens is presented in Fig. 1. The black phase is graphite and the dark gray phase is SiC, which both appear to be uniformly distributed in the lighter colored ZrB_2 phase. SEM observations did not show any indication of porosity, which was consistent with the density values measured by the Archimedes technique. Graphite flakes seemed to be oriented preferentially perpendicular to the hot pressing direction. Based on SEM observations and density measurements, porosity is not expected to have a significant effect on the oxidation behavior.

3.2. Oxide scale morphology

Similar to ZrB_2–SiC, a layered structure formed during oxidation of ZrB_2–SiC–C at 1500 °C in air.[21,30] The layered structure (Fig. 2) consisted of (1) a uniform SiO_2-rich layer on the surface, (2) a layer of ZrO_2 and SiO_2 (ZrO_2–SiO_2), (3) a layer of ZrO_2, (4) a partially oxidized layer composed of ZrO_2, ZrB_2, and graphite, and (5) the unaffected ZrB_2–SiC–C. Due to the formation of a stable SiO_2-rich layer, ZrB_2–SiC–C is expected to exhibit passive oxidation behavior with parabolic mass gain kinetics at 1500 °C, similar to what has been reported for ZrB_2–SiC.[30] The protective SiO_2-rich layer should inhibit the diffusion of oxygen to the underlying ZrB_2–SiC–C. Beneath the SiO_2-rich layer was a thin layer containing ZrO_2 and SiO_2 and a thin layer of ZrO_2. Next was the partially oxidized layer. Some SiC may remain in this layer, although it was not detected by XRD and the thermodynamic analysis discussed below will show that SiC may not be stable, while graphite appears to be stable, in this layer. Analysis by EDS verified the presence of carbon in the partially oxidized layer (Fig. 2). For the SEM images, graphite is the darkest phase (Figs. 1 and 2a) whereas EDS maps are brighter in areas that are rich in the selected element (Fig. 2b–e). Because the thicknesses of the outer SiO_2-rich layer and the ZrO_2–SiO_2 layer varied and the boundary between the two was not sharp, a combined label was used to identify them in Fig. 2a. Also the sample was charged slightly during collection of EDS map and as a result it could appear that it drifted, however, the analysis still provides a clear picture of the phase distribution.

Grazing X-ray diffraction was used to identify the crystalline phases present in the reaction layers. A specimen oxidized at 1500 °C for 8 h was used for this study to maximize the thickness of the layers. The top layer, as indicated by SEM and EDS discussed above, was composed of a SiO_2-rich glassy layer. This layer was ~5 μm thick after oxidation in air at 1500 °C for 30 min and grew to ~20 μm after 8 h. Since this layer did not contain any crystalline phases, it was not examined using GXRD. Below the amorphous surface layer were a thin layer of ZrO_2–SiO_2 and a thin layer of crystalline ZrO_2 (Fig. 3). Together these two layers were ~2 μm thick after 30 min and ~8 μm thick after 8 h. No graphite peaks were observed in these layers by GXRD or and no graphite was detected during SEM/EDS analysis. The structure and composition of the SiO_2-rich, ZrO_2-SiO_2, and ZrO_2 layers are similar to what has been analyzed for ZrB_2–SiC[6,8,21,30] and, consequently, will not be discussed in detail in this paper.

Beneath the ZrO_2 layer, a partially oxidized layer was identified. This layer had a porous structure from which SiC has been partially or entirely removed. In contrast to what has been observed for oxidation of ZrB_2–SiC, this layer contained a significant amount of graphite. The morphology of the grains in this region was similar to the original structure before oxidation, except that the SiC has been partially or fully removed, presumably by active oxidation. It appears that some additional carbon may have deposited in this layer as the SiC was removed, a phenomenon that has been reported in a few previous studies, but that has not been evaluated thermodynamically.[36] The SiC could be removed either by direct volatilization to SiO (g) and CO (g) or by oxidation of SiC to SiO_2 (c)[2] followed by the active reduction of SiO_2 (c) to SiO (g) due to low oxygen

[2] (c) stands for a condensed phase.

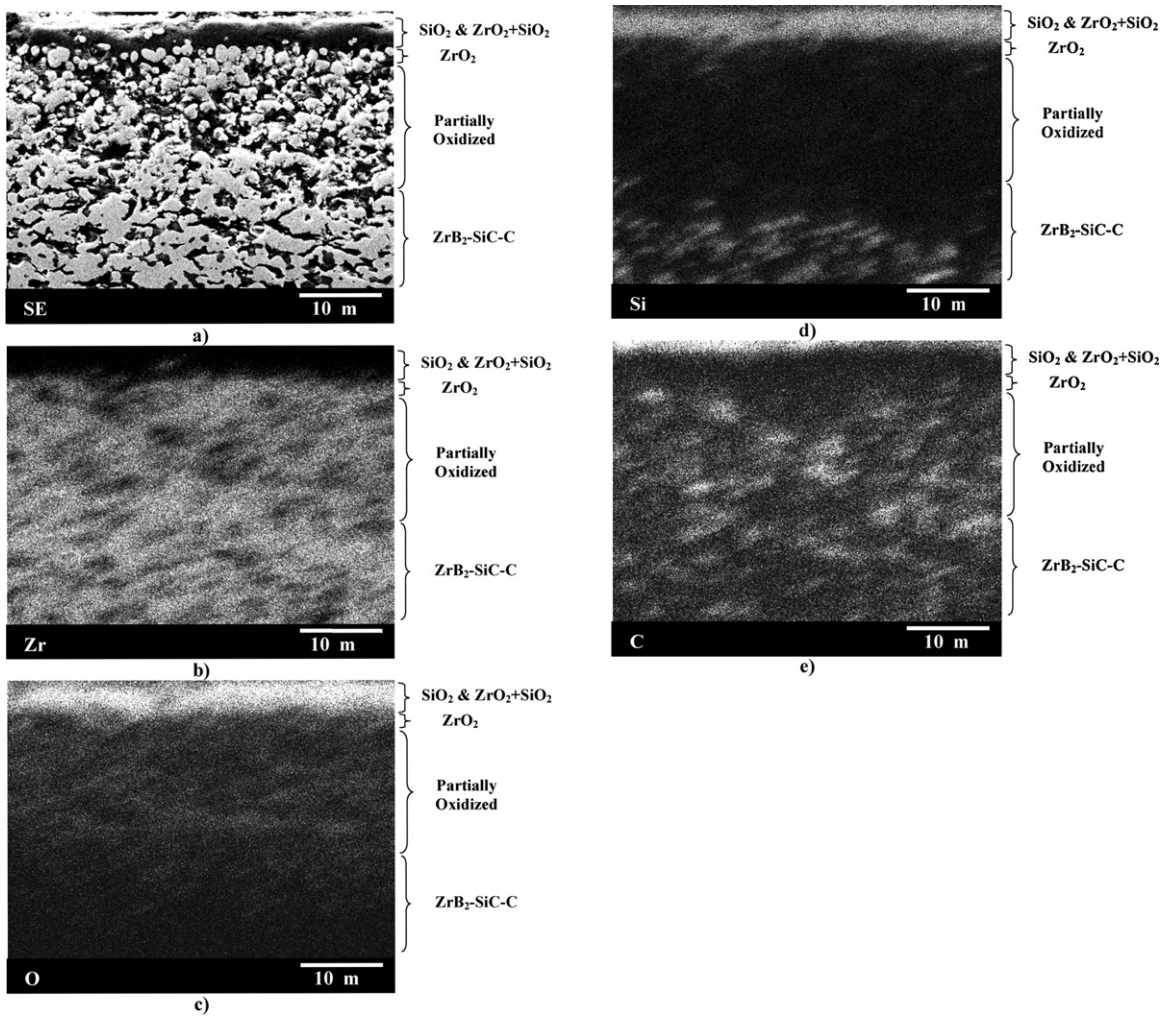

Fig. 2. A polished cross section of ZrB_2–SiC–C that was oxidized in air at 1500 °C for 30 min showing (a) a SEM micrograph and EDS compositional maps for (b) Zr, (c) O, (d) Si, and (e).

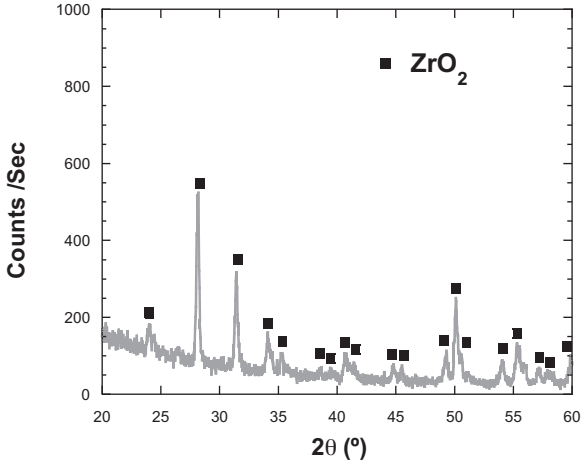

Fig. 3. Grazing incidence X-ray diffraction analysis of the ZrO_2–SiO_2 layer just beneath the SiO_2 rich surface layer in ZrB_2–SiC–C oxidized in air at 1500 °C for 8 h showing that ZrO_2 was the only crystalline phase present.

pressure in this region. The thickness of the partially oxidized layer was more than 20 μm after heating to 1500 °C for 30 min (Fig. 2) and it grew to ~40 μm after heating to 1500 °C for 8 h. In the upper part of this region near the ZrO_2–SiO_2 layer, GXRD detected ZrO_2 and graphite (Fig. 4), while ZrO_2, ZrB_2 and graphite were detected deeper in the layer near the interface with the unaffected ZrB_2–SiC–C (Fig. 5). No SiC was detected in this region. Although a distinct interface separating a ZrO_2 + C layer from a ZrB_2 + C layer might be expected in the partially oxidized region, none was observed by SEM or GXRD analysis suggesting a graded structure that transitioned from ZrO_2 and graphite in the upper regions to ZrO_2, ZrB_2, and graphite in the lower regions.

The addition of graphite to ZrB_2-SiC did not affect the thickness of SiO_2-rich layer or ZrO_2–SiO_2 layer, but increased the thickness of partially oxidized layer. Compared to common ZrB_2–SiC ceramics, the partially oxidized layer is about twice as thick in ZrB_2–SiC–C.[37] The increased thickness of this layer could be due to the fact that only 15 vol.% SiC used in ZrB_2–SiC–C versus 30 vol.% used in the material in the reference study. No effect was found on morphology of newly formed

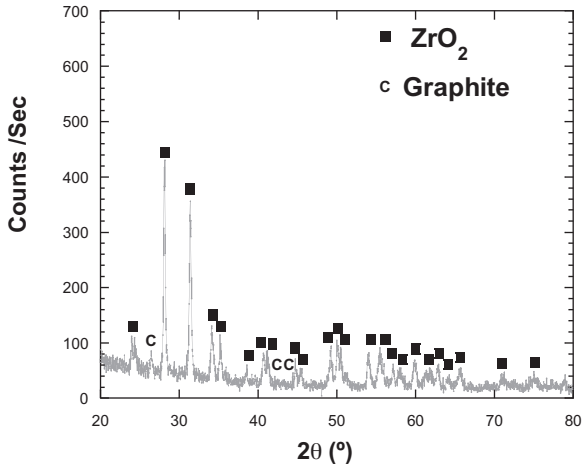

Fig. 4. Grazing incidence X-ray diffraction analysis of the partially oxidized layer just beneath the ZrO_2–SiO_2 layer in ZrB_2–SiC–C oxidized in air at 1500 °C for 8 h showing that ZrO_2 and graphite were present in this region.

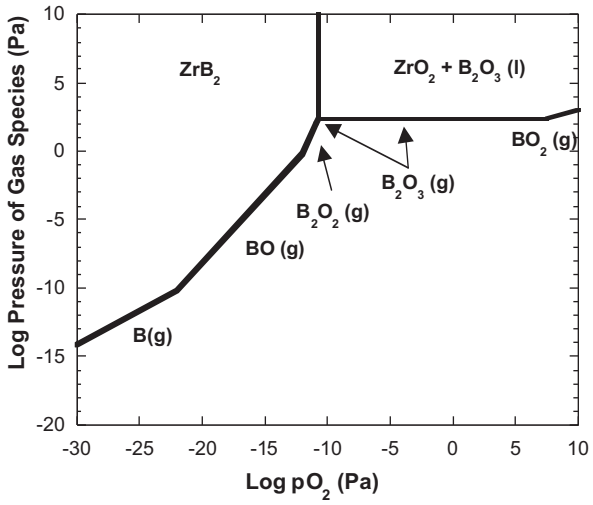

Fig. 6. A volatility diagram for ZrB_2 at 1500 °C.

phases as a result of addition of graphite. Due to the increased thickness of the partially oxidized layer, the gradient of oxygen activity across the partially oxidized layer may be less severe compared to the original ZrB_2–SiC.

3.3. Thermodynamic analysis

Volatility diagrams are isothermal plots showing the pressure of the predominant gaseous species as a function of oxygen pressure in equilibrium with the various condensed phases that are stable in the system.[38] These diagrams are useful tools for presenting thermodynamic data in a way that can be used to understand the chemistry of high temperature gas–solid interactions such as oxidation.[38] Volatility diagrams have been constructed for oxides such as MgO, Al_2O_3, and SiO_2[38] as well as non-oxide ceramics such as SiC and Si_3N_4.[39] In the current study, volatility diagrams were constructed for ZrB_2, SiC, and graphite to investigate the stability of graphite in the partially oxidized region of the oxidized ZrB_2–SiC specimen and to determine the reaction sequences that resulted in the development of the layered structure. A commercial thermodynamic software package (FactSage® 5.4, Thermofact Ltd., Montreal, Canada) using Fact compound database was employed as the source of the thermodynamic data for constructing the volatility diagrams.

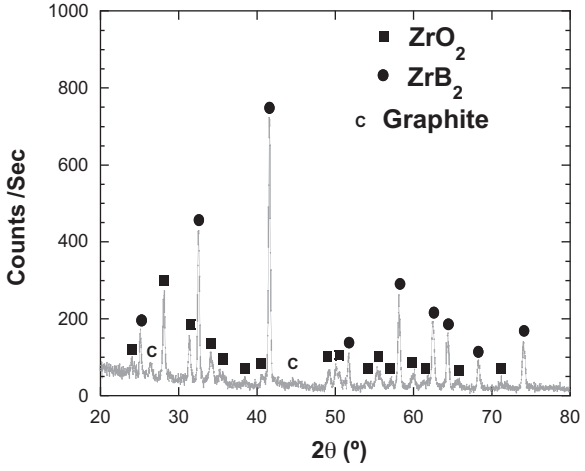

Fig. 5. Grazing incidence X-ray diffraction analysis of the partially oxidized layer formed near the unoxidized ZrB_2–SiC–C in a specimen oxidized in air at 1500 °C for 8 h. ZrO_2, graphite, and ZrB_2 were present.

3.3.1. The ZrB_2 volatility diagram at 1500 °C

A volatility diagram for ZrB_2 has been described previously.[22] The ZrB_2 volatility diagram based on the earlier report was constructed for this study (Fig. 6) and shows that the equilibrium pO_2 for the transition of ZrB_2 to $ZrO_2 + B_2O_3$ (l) (Reaction (1)) is 1.9×10^{-11} Pa ($\log pO_2 = -10.73$). Below the transition pO_2, the vapor species are in equilibrium with ZrB_2.

$$ZrB_2 + 5/2O_2(g) \rightarrow ZrO_2 + B_2O_3(l) \quad (1)$$

3.3.2. The SiC volatility diagram at 1500 °C

Various SiC volatility diagrams have been reported in the literature.[21,39–41] In the current study, a modified diagram was produced since it was assumed that the presence of graphite increased the activity of carbon to one in all cases, which would make CO (g) the predominant gaseous species. The equilibrium module of the thermodynamic software showed that when a mixture of ZrB_2, SiC, and graphite was exposed to a limited amount of oxygen, the major constituent of the gaseous phase was CO (g) (>99% of gaseous phase), which was present in a significantly higher amount than SiO (g) (<1%). Therefore, the pressure of CO (g) was assumed to be constant at $pCO = 1.013 \times 10^5$ Pa (1 atm) for the SiC volatility diagram calculated for the present study. A similar diagram for SiC has been reported by Heuer and Lou.[39] The present calculation assumed that SiC was in its alpha (hexagonal or rhombohedral) polymorph since α-SiC was used as the precursor for fabrication of the ZrB_2–SiC–C specimens. The SiC volatility diagram (Fig. 7) shows that the pO_2 for the equilibrium transition from SiC to SiO_2 + graphite (Reaction (2)) is 1.3×10^{-11} Pa

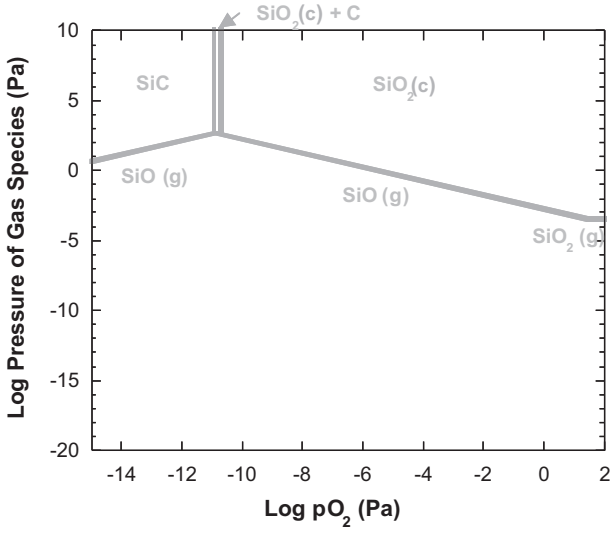

Fig. 7. A volatility diagram for SiC at 1500 °C assuming $pCO = 1.013 \times 10^5$ Pa.

($\log pO_2 = -10.90$). Above $pO_2 = 2.0 \times 10^{-11}$ Pa, graphite is no longer stable and reacts to form CO (g) (Reaction (3)). Below $pO_2 = 30$ Pa, the predominant vapor species in equilibrium with SiO_2 (c) is SiO (g). Above $pO_2 = 30$ Pa, SiO_2 (g) is the predominant gas species in equilibrium with SiO_2 (c).

$$SiC + O_2(g) \rightarrow SiO_2(c) + C \quad (2)$$

$$C + \tfrac{1}{2}O_2 \rightarrow CO(g) \quad (3)$$

3.3.3. Graphite stability

Thermodynamic calculations indicated that at 1500 °C and a total pressure of carbon monoxide of $pCO = 1.013 \times 10^5$ Pa (1 atm), graphite is stable below $pO_2 = 2.0 \times 10^{-11}$ Pa ($\log pO_2 = -10.70$). At $pO_2 = 2.0 \times 10^{-11}$ Pa or above, graphite reacts with oxygen to form CO (g) (Reaction (3)). The transition equilibrium pO_2 for conversion of graphite to carbon monoxide is represented as a vertical line ($\log pO_2 = -10.70$) in the SiC volatility diagram (Fig. 7).

3.3.4. Formation of the layered structure

To understand the thermodynamic stability of the layered structure that developed when ZrB_2–SiC–C was exposed to air at 1500 °C, a combined volatility diagram (Fig. 8) was constructed by overlapping the volatility diagrams for ZrB_2 and SiC. All of the discussions for the stability of the formation of the layered structure are based on the assumption that an oxygen pressure gradient formed across the layered structure with the highest pO_2 at the outer surface and the pO_2 decreasing as the depth into the specimen increased.[21] Based on the combined volatility diagram, oxidation of graphite to CO (g) occurs at $pO_2 = 2.0 \times 10^{-11}$ Pa ($\log pO_2 = -10.70$). The next transition occurs at an oxygen pressure of 1.9×10^{-11} Pa ($\log pO_2 = -10.73$), where ZrB_2 transforms to $ZrO_2 + B_2O_3$ (l) by Reaction (1). Both ZrB_2 and the oxidized products (ZrO_2 and B_2O_3 (l)) have a high vapor pressure of B_2O_3 ($pB_2O_3 = 2.7 \times 10^3$ Pa) near the transition pO_2, although ZrB_2

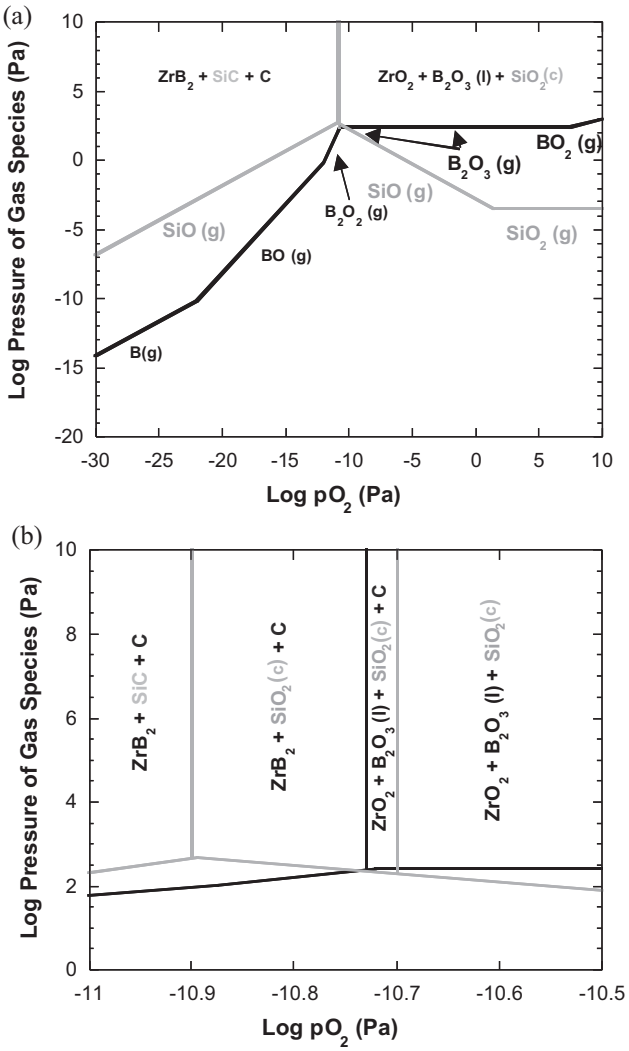

Fig. 8. A combined volatility diagram for ZrB_2, SiC, and graphite at 1500 °C ($pCO = 1.013 \times 10^5$ Pa), (a) over a large range of pO_2 (b) expanded to show the pO_2 range of interest.

does not exhibit weight loss since the ZrO_2 formed by oxidation is stable and remains on the surface. At $pO_2 = 1.3 \times 10^{-11}$ Pa ($\log pO_2 = -10.90$ Pa), SiC reacts to form SiO_2 and graphite by Reaction (2). As with ZrB_2, both SiC and SiO_2 have a high vapor pressure of SiO (g) near the transition pO_2 ($pSiO = 4.8 \times 10^2$ Pa for both SiC and SiO_2 at $pO_2 = 1.3 \times 10^{-11}$ Pa). Hence, SiC undergoes rapid weight loss near the transition pO_2 due to either active oxidation of SiC below the transition pO_2 (SiO (g) and C (s) are produced) or passive oxidation with rapid evaporation of the SiO_2 (c) above the transition pO_2 (SiO_2 (c) and C (s) produced, but the SiO_2 (c) vaporizes due to high vapor pressure of SiO (g)). Below $pO_2 = 1.3 \times 10^{-11}$ Pa ($\log pO_2 = -10.90$ Pa), ZrB_2, SiC, and graphite are all stable.

From the combined volatility diagram (Fig. 8a), exposure of ZrB_2–SiC–C to air ($pO_2 = 2.0 \times 10^4$ or $\log pO_2 = 4.31$) at 1500 °C should result in the formation of $ZrO_2 + B_2O_3$ (l) + SiO_2 (c). The vapor pressure of B_2O_3 (g) is several orders of magnitude greater than any other species and is high enough

($pB_2O_3 = 2.7 \times 10^3$ Pa in air) that B_2O_3 vaporizes preferentially by Reaction (4) at this temperature.[20]

$$B_2O_3(l) \rightarrow B_2O_3(g) \quad (4)$$

Boron deficiency of the outer SiO_2 (c) layer was confirmed experimentally for ZrB_2–SiC using secondary ion mass spectrometry (SIMS), which showed that the surface layer contained less than 1 wt.% boron.[20] This indicated that B_2O_3 was depleted from the borosilicate glass, probably due to preferential evaporation because of its high vapor pressure relative to SiO_2.[20] Additional studies have reported that only a limited amount of ZrO_2 is produced during the initial heating of ZrB_2–SiC to 1500 °C before the SiC starts to oxidize.[37] These studies have reported that the ZrO_2 that was formed during the initial heating was contained in a ZrO_2–SiO_2 layer, which remained near the underlying ZrB_2-containing material, and ZrO_2 was not present at the outer surface. Thus, a SiO_2-rich layer was observed on top of a ZrO_2–SiO_2 layer when ZrB_2–SiC was oxidized, similar to other literature reports.[6,8,21,30] A similar structure consisting of a SiO_2-rich outer layer and a ZrO_2–SiO_2 layer was observed for the oxidation of ZrB_2–SiC–C in the present study.

Experimentally, a layer of ZrO_2 was observed beneath the ZrO_2–SiO_2 layer (Figs. 2 and 3) when ZrB_2–SiC–C was oxidized at 1500 °C. Formation of a ZrO_2 layer is consistent with thermodynamic equilibrium calculations. Since no graphite was found in this layer, the pO_2 should be greater than 2.0×10^{-11} Pa ($\log pO_2 > -10.70$), which support oxidation of graphite to CO (g). According to the combined volatility diagrams (Fig. 8a and b), if ZrB_2–SiC–C is exposed to any oxygen pressure from $pO_2 > 2.0 \times 10^{-11}$ Pa ($\log pO_2 > -10.70$) up to the pressure of oxygen present in air at 1500 °C, $ZrO_2 + B_2O_3$ (l) + SiO_2 (c) should form. In this range of oxygen pressures, B_2O_3 (l) has a high vapor pressure ($pB_2O_3 = 2.7 \times 10^3$ Pa) and is not likely to exist as a stable condensed species in an open system. Any B_2O_3 (l) produced in this region would likely evaporate and be transported to the SiO_2-containing layer on the surface where it would dissolve into the glass, diffuse to the outer surface, and be removed from the system. Similarly, the SiO_2 (c) can be removed from this layer. Because of the low pO_2, SiO_2 (c) has a high vapor pressure of SiO (g) ($pSiO > 1.0 \times 10^2$ Pa), which means that it can evaporate, be transported to the outer SiO_2-containing layers, and condense back to SiO_2 (c) to increase the thickness of these layers. Because these are chemical reactions, the equilibrium pressure of oxygen and the equilibrium vapor pressure of SiO (g) can be calculated at the interfaces where the species are produced and consumed, if some assumptions are made. Since both pO_2 and pSiO are not known, but are interdependent, one or the other must be assumed so that the rest of the calculations can be completed. For this study, a value of $pSiO = 1.0 \times 10^2$ Pa at the interface between the ZrO_2–SiO_2 layer and the ZrO_2 layers was assumed as the pressure at which SiO (g) would condense to SiO_2 (c). This value is similar to the value of $pSiO = 4.0 \times 10^2$ Pa calculated in another study for the condensation of SiO (g) to SiO_2 (c) at the interface of the SiC-depleted layer and ZrO_2–SiO_2 layer when ZrB_2–SiC was exposed to air at 1500 °C.[21] Based on this value of pSiO, the activity of oxygen at this interface was calculated to be $pO_2 = 2.9 \times 10^{-10}$ Pa ($\log pO_2 = -9.54$). Based on the pSiO assumed for the interface between the ZrO_2–SiO_2 layer and the ZrO_2 layer and the criterion for graphite stability, the ZrO_2 layer should have oxygen pressures that range from 2.0×10^{-11} Pa to 2.9×10^{-10} Pa ($\log pO_2$ from −10.70 to −9.54).

$$SiO_2(c) \rightarrow SiO(g) + \tfrac{1}{2}O_2(g) \quad (5)$$

Experimentally, a partially oxidized layer composed of ZrO_2, ZrB_2, and graphite was observed by SEM and XRD analysis beneath the ZrO_2 layer. According to the volatility diagram (Figs. 7 and 8b), the pressure of oxygen should be below 2.0×10^{-11} Pa ($\log pO_2 < -10.70$) in this layer based on the stability criterion for graphite. Oxygen pressure should decrease across the layer due to the gradient associated with the diffusion profile. At the lower end of this layer, the interface between the partially oxidized layer and the unoxidized ZrB_2–SiC–C, the pO_2 must be less than 1.9×10^{-11} Pa ($\log pO_2 > -10.73$) since ZrB_2 is observed in this region. In addition, the pO_2 at this interface may also be below the equilibrium pO_2 for SiC–SiO_2 (Reaction (2)), which is 1.3×10^{-11} Pa ($\log pO_2 < -10.90$). If the pO_2 was greater than 1.3×10^{-11} Pa, then a layer of SiO_2 (c) would form on the surface of the ZrB_2–SiC–C layer, which would be reduced to SiO (g) and be transported across the partially oxidized layer and ZrO_2 layer.[21] Assuming that $pO_2 = 1.3 \times 10^{-11}$ Pa at this interface, then pSiO can be calculated to be $pSiO = 4.8 \times 10^2$ Pa based on the equilibrium established by Reaction (5). It seems more likely that the pO_2 is less than 1.3×10^{-11} Pa at this interface since no condensed SiO_2 is observed there. Based on the volatility diagram for SiC presented in Fig. 7, the pSiO in equilibrium with SiC decreases as pO_2 decreases. In addition, a pSiO gradient must be maintained across the partially oxidized and ZrO_2 layers to maintain a driving force for diffusion of SiO (g) from where it is generated at the upper edge of the ZrB_2–SiC–C layer to where it is consumed at the lower edge of the ZrO_2–SiO_2 layer. Based on the decrease of pSiO with pO_2 in equilibrium with SiC, the pSiO cannot be lower than 1.0×10^2 Pa, its value at the interface of the ZrO_2–SiO_2 and ZrO_2 layers to maintain a chemical potential gradient to drive transport of SiO (g) across the partially oxidized and ZrO_2 layers. Using $pSiO = 1.0 \times 10^2$ Pa as the lower limit, the minimum pO_2 was calculated to be 5.5×10^{-13} Pa for SiC–SiO equilibrium (Reaction (6)).

$$SiC + \tfrac{1}{2}O_2(g) \rightarrow SiO(g) + C \quad (6)$$

The range of pressures of oxygen calculated for formation and stability of the partially oxidized layer (5.5×10^{-13} Pa < pO_2 < 2.0×10^{-11} Pa) corresponds to three regions in the combined volatility diagram (Fig. 8b). These three regions are: (1) 1.9×10^{-11} Pa < pO_2 < 2.0×10^{-11} Pa ($-10.73 < \log pO_2 < -10.70$) in which the stability of $ZrO_2 + B_2O_3$ (l) + SiO_2 (c) + C is favorable; (2) 1.3×10^{-11} Pa < pO_2 < 1.9×10^{-11} Pa ($-10.90 < \log pO_2 < -10.73$) in which the stability of $ZrB_2 + SiO_2$ (c) + C is favorable; and (3) 5.5×10^{-13} Pa < pO_2 < 1.3×10^{-11} Pa ($-12.26 < \log pO_2 < -10.90$) in which $ZrB_2 + SiC + C$ are

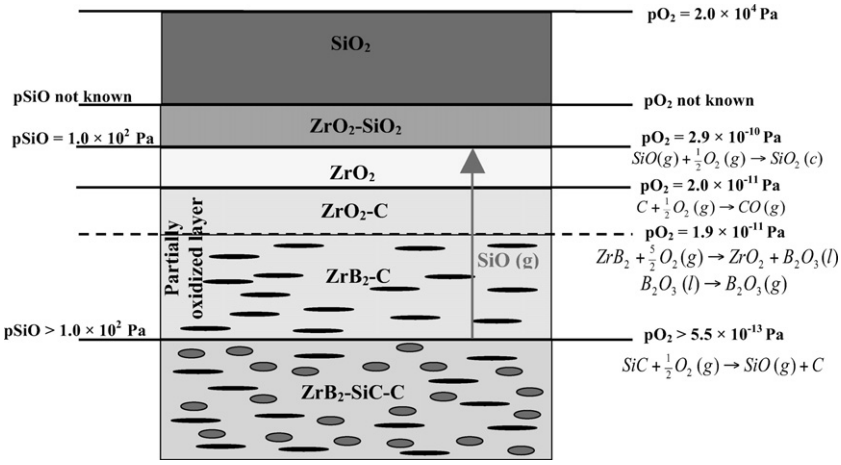

Fig. 9. A model showing the composition of the layers in the structure formed after oxidation of ZrB_2–SiC–C in air at 1500 °C along with the chemical process that are active, and the calculated oxygen and SiO (g) pressures.

stable and no new condensed phases are expected to form. In all three regions (5.5×10^{-13} Pa < pO_2 < 2.0×10^{-11} Pa), neither B_2O_3 (l) nor SiO_2 (c) were observed as condensed phases, presumably due to their volatility. As discussed earlier, B_2O_3 (g) and SiO (g) were formed, transported across the partially oxidized layer, and then condensed in the SiO_2-containing ZrO_2–SiO_2 layer. Likewise, SiC is also expected to be removed from this region through active oxidation (Reaction (6)) due to the formation of SiO (g). Vaporization of B_2O_3 (l) and active reduction of SiO_2 (c) from the layer where $ZrO_2 + B_2O_3$ (l) + SiO_2 (c) + C were predicted as condensed phases resulted in the formation of a region containing ZrO_2 and C. Active reduction of SiO_2 (c) from the region where $ZrB_2 + SiO_2$ (c) + C were stable resulted in the formation of a region containing ZrB_2 and C. Active oxidation of SiC from the unoxidized ZrB_2 + SiC + C could also increase the thickness of the region containing ZrB_2 and C. As discussed earlier, no distinct interface was observed between the ZrB_2 + C and ZrO_2 + C layers. Rather a graded structure that was composed of ZrO_2 + C at the top and ZrB_2 + C at the bottom appears to have formed.

A model that schematically represents the likely oxygen pressures and chemical process predicted to be active in the structure produced during oxidation of ZrB_2–SiC–C at 1500 °C in air is shown in Fig. 9. The surface protective layers can only grow with time if some Si-containing species is transported to this layer from an underlying layer. Because of the formation of the partially oxidized region that is free of Si-containing species, continued active oxidation of SiC (Reaction (6)) at the upper interface of the unoxidized ZrB_2–SiC–C and the subsequent transport of SiO (g) from the SiC-containing layer to the ZrO_2–SiO_2 layer is required. From the microstructural and thermodynamic analysis, the addition of graphite does not inhibit the formation of a partially oxidized layer. Further, based on the oxygen activities below the outer SiO_2-rich scale, suppression of the formation of a partially oxidized layer may not be possible in SiC-containing diboride systems.

4. Summary

Specimens of ZrB_2 containing 15 volume percent SiC and 15 volume percent graphite were oxidized in a flowing air at 1500 °C. A layered structure was formed on the surface during exposure. Graphite was found to be stable in a porous partially oxidized layer below the SiO_2-rich surface layer. A combined volatility diagram for ZrB_2, SiC, and graphite was used to justify, on a thermodynamic basis, the development of the layered structure and stability of graphite in the partially oxidized layer. The active oxidization of SiC and/or its oxidation to SiO_2 (c) and then reduction to SiO (g) at the reducing conditions thought to exist under the external layer of SiO_2 leads to the removal of SiC from a layer that contains ZrO_2, ZrB_2, and graphite. Silicon containing phases are not stable in the partially oxidized layer due to the high vapor pressure of SiO in reducing conditions. Based on the fact that graphite is stable in the partially oxidized layer, the pO_2 in this region was calculated to be less than 2.0×10^{-11} Pa. Using the thermodynamic conditions needed to drive the transport of SiO (g) from the SiC in the unoxidized ZrB_2–SiC–C, across the partially oxidized region, and to ZrO_2–SiO_2 layer, the lower limit of pO_2 in the partially oxidized layer was calculated to be 5.5×10^{-13} Pa. In air at 1500 °C, ZrB_2–SiC–C should exhibit passive oxidation with diffusion controlled kinetics due to the protection provided by the stable SiO_2 scale on the surface even though SiC undergoes active oxidation beneath the protective outer scale resulting in the formation of a porous partially oxidized layer between the outer scale and the underlying unoxidized ZrB_2–SiC–C.

References

1. Levine SR, Opila EJ, Halbig MC, Kiser JD, Singh M, Salem JA. Evaluation of ultra high temperature ceramics for aeropropulsion use. *J Eur Ceram Soc* 2002;**22**:2757–67.
2. Monteverde F, Bellosi A. Development and characterization of metal–diboride-based composites toughened with ultra-fine SiC particulates. *Solid State Sci* 2005;**7**:622–30.

3. Monteverde F, Bellosi A. The resistance to oxidation of an HfB_2–SiC composite. *J Eur Ceram Soc* 2005;**25**:1025–31.
4. Opeka MM, Talmy IG, Zaykoski JA. Oxidation-based materials selection for 2000°C + hypersonic aerosurfaces: theoretical considerations and historical experience. *J Mater Sci* 2004;**39**(19):5887–904.
5. Van Wie DM, Drewry Jr DG, King DE, Hudson CM. The hypersonic environment: required operating conditions and design challenges. *J Mater Sci* 2004;**39**(19):5915–24.
6. Chamberlain AL, Fahrenholtz WG, Hilmas GE. Oxidation of ZrB_2–SiC ceramics under atmospheric and reentry conditions. *Refract Appl Trans* 2005;**1**(2):1–8.
7. Sciti D, Brach M, Bellosi A. Oxidation behavior of a pressureless sintered ZrB_2–$MoSi_2$ ceramic composite. *J Mater Res* 2005;**20**(4):922–30.
8. Monteverde F, Bellosi A. Oxidation of ZrB_2-based ceramics in dry air. *J Electrochem Soc* 2003;**150**(11):B552–9.
9. Nguyen QN, Opila EJ, Robinson RC. Oxidation of ultra high temperature ceramics in water vapor. *J Electrochem Soc* 2004;**151**(10):B558–62.
10. Bartulli C, Valente T, Tului M. High temperature behavior of plasma sprayed ZrB_2–SiC composite coatings. In: *Thermal Spray 2001: New Surfaces for a New Millennium Proceedings of the International Thermal Spray Conference, Singapore*. Materials Park, OH, USA: ASM International; 2001. p. 259–62.
11. Valente T, Mariano G, Tului M. Mechanical properties of ceramic matrix composite for high temperature applications obtained by plasma spraying. In: *Thermal Spray 2004: Advances in Technology and Application, Proceedings of the International Thermal Spray Conference*. Materials Park, OH, USA: ASM International; 2001. p. 32–5.
12. Monteverde F, Bellosi A, Guicciardi S. Processing and properties of zirconium diboride-based composites. *J Eur Ceram Soc* 2002;**22**:279–88.
13. Cutler RA. Engineering properties of borides. In: Schneider Jr SJ, editor. *Ceramics and Glasses, Engineered Materials Handbook*, vol. 4. Materials Park, OH: ASM International; 1991. p. 787–803.
14. Berkowitz-Mattuck JB. High-temperature oxidation: III. Zirconium and hafnium diborides. *J Electrochem Soc* 1966;**113**(9):908–14.
15. Kuriakose AK, Margrave JL. The Oxidation kinetics of zirconium diboride and zirconium carbide at high temperatures. *J Electrochem Soc* 1964;**111**(7):827–331.
16. Tripp WC, Graham HC. Thermogravimetric study of the oxidation of ZrB_2 in the temperature range of 800–1500 °C. *J Electrochem Soc* 1968;**118**(7):1195–9.
17. Irving RJ, Worsley IG. Oxidation of titanium diboride and zirconium diboride at high temperatures. *J Less-Common Met* 1968;**16**(2):102–12.
18. Khanra AK. Oxidation behavior of zirconium diboride. *J Aust Ceram Soc* 2003;**39**(2):114–8.
19. Brach M, Sciti D, Balbo A, Bellosi A. Short-term oxidation of a ternary composite in the system AlN–SiC–ZrB_2. *J Eur Ceram Soc* 2005;**25**(10):1771–80.
20. Rezaie AR, Fahrenholtz WG, Hilmas GE. Oxidation of zirconium diboride–silicon carbide at 1500 °C in a low partial pressure of oxygen. *J Am Ceram Soc* 2006;**89**(10):3240–5.
21. Fahrenholtz WG. Thermodynamic analysis of ZrB_2–SiC oxidation: formation of a SiC-depleted region. *J Am Ceram Soc* 2007;**90**(1):143–8.
22. Fahrenholtz WG. The ZrB_2 volatility diagram. *J Am Ceram Soc* 2005;**88**(12):3509–12.
23. Bundschuh K, Schuze M, Muller C, Greil P, Heider W. Selection of materials for use at temperatures above 1500 °C in oxidizing atmospheres. *J Eur Ceram Soc* 1998;**18**:2389–91.
24. Pankov GA, Fomina GA, Ivanov DA, Val'yano GE. Strength and scaling resistance of a composite based on zirconium diboride. *Refractories* 1994;**35**(9–10):298–300.
25. Kobayashi K, Sano H, Maeda K, Uchiyama Y. Oxidation behavior of graphite–B_4C/SiC/ZrB_2 composite in dry and moist atmosphere. *J Ceram Soc Jpn Int Ed* 1992;**100**:407–11.
26. Zhong X, Zhao H. High temperature properties of refractory composites. *Am Ceram Soc Bull* 1999;**78**:98–101.
27. Tripp WC, Davis HH, Graham HC. Effect of an SiC addition on the oxidation of ZrB_2. *Am Ceram Soc Bull* 1973;**52**(8):612–3.
28. Opila E, Levine S, Lorincz J. Oxidation of ZrB_2- and HfB_2-based ultra-high temperature ceramics: effect of Ta additions. *J Mater Sci* 2004;**39**(19):5969–77.
29. Gasch M, Ellerby D, Irby E, Beckman S, Gusman M, Johnson S. Processing, properties, and arc jet oxidation of hafnium diboride/silicon carbide ultra high temperature ceramics. *J Mater Sci* 2004;**39**(19):5925–37.
30. Opila EJ, Halbig MC. Oxidation of ZrB_2–SiC. *Ceram Eng Sci Proc* 2001;**22**(3):221–8.
31. Clougherty EV, Pober RL, Kaufman L. Synthesis of oxidation resistance metal diboride composites. *Trans Metall Soc AIME* 1968;**242**:1077–82.
32. Luthra KL. Some new perspective on oxidation of silicon carbide and silicon nitride. *J Am Ceram Soc* 1991;**74**(5):1095–103.
33. Jacobson NS, Lee KN, Fox DS. Reactions of silicon carbide and silicon (IV) oxide at elevated temperatures. *J Am Ceram Soc* 1992;**75**(6):1603–11.
34. Chamberlain AL, Fahrenholtz WG, Hilmas GE, Ellerby DT. High strength ZrB_2-based ceramics. *J Am Ceram Soc* 2004;**87**(6):1170–2.
35. Rezaie AR, Fahrenholtz WG, Hilmas GE. Effect of hot pressing time and temperature on the microstructure and mechanical properties of ZrB_2–SiC. *J Mater Sci* 2007;**42**(8):2735–44.
36. Monteverde F. Beneficial effects of ultra-fine α-SiC incorporated on the sinterability and mechanical properties of ZrB_2. *Appl Phys A* 2006;**82**:329–37.
37. Rezaie AR, Fahrenholtz WG, Hilmas GE. Evolution of Structure During the Oxidation of Zirconium Diboride-Silicon Carbide in Air up to 1500 (C. *J Eur Ceram Soc* 2007;**27**(6):2495–501.
38. Lou VLK, Mitchell TE, Heuer AH. Review – graphical displays of the thermodynamics of high temperature gas–solid reactions and their application to oxidation of metals and evaporation of oxides. *J Am Ceram Soc* 1985;**68**(2):49–58.
39. Heuer AH, Lou VLK. Volatility diagrams for silica, silicon nitride, and silicon carbide and their application to high temperature decomposition and oxidation. *J Am Ceram Soc* 1990;**73**(10):2789–803.
40. Schneider B, Guette A, Naslain R, Cataldi M, Costecalde A. Theoretical and experimental approach to the active-to-passive transition in the oxidation of silicon carbide experiments at high temperatures and low total pressures. *J Mater Sci* 1998;**33**(2).
41. Jacobson NS. Corrosion of silicon–based ceramics in combustion environments. *J Am Ceram Soc* 1993;**76**(1):3–28.